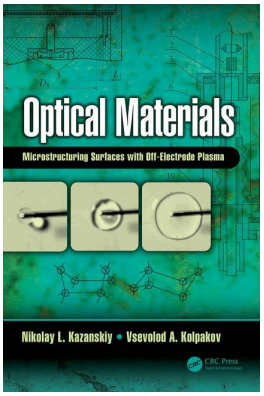


# Optical Materials
# Microstructuring Surfaces with Off-Electrode Plasma

Nikolay L. Kazanskiy, Vsevolod A. Kolpakov

## Increasing the Degree of Surface Cleanliness with Low-Temperature Off-Electrode Plasma

Publication details
https://www.routledgehandbooks.com/doi/10.1201/b21918-3
Nikolay L. Kazanskiy, Vsevolod A. Kolpakov
**Published online on: 23 Mar 2017**

# 3 Increasing the Degree of Surface Cleanliness with Low-Temperature Off-Electrode Plasma

A major problem hindering the development of diffractive optics and micro- and nanoelectronics is how to fabricate surfaces with the desired degree of cleanliness. Residual resist layers as well as organic molecular compounds (solvents, chemicals, etc.) adsorbed at wafer surfaces are the primary sources of contamination [160,161]. This necessitates cleaning organic contaminants off substrate surfaces before etching.

Today, the most common surface-cleaning techniques are chemical cleaning, laser cleaning, and plasma cleaning. To generate uniform plasma, plasma techniques use high-frequency (HF) and superhigh-frequency (SHF) sources that are complex, costly, and energy-intensive. Treating wafers with plasma generated by such sources contaminates surfaces with low-active or inactive particles because the substrate is placed between the electrodes of the gas-discharge device. Plasma parameters in this case are determined chiefly by the properties of the surface being treated (the loading effect).

Chapter 1 demonstrated the advantages of using off-electrode plasma. In that technique, ion-plasma fluxes are formed outside the electrodes, and the possibility of the surface becoming contaminated with inactive plasma particles is ruled out because only negatively charged particles (ions and electrons) move toward the surface. But because contemporary literature is silent on theoretical and experimental research into the mechanism of surface cleaning that uses off-electrode plasma, no practical methods are yet available.

This chapter analyses widely used conventional cleaning techniques and theoretically and experimentally investigates the mechanism of surface cleaning with directed fluxes of low-temperature plasma generated by a high-voltage gas discharge outside the electrode gap. The discussion is aimed at creating efficient cleaning methods to improve the fabrication quality of optical microreliefs.

## 3.1 OVERVIEW OF METHODS FOR SURFACE CLEANING

The major difficulty in forming a mask during the fabrication of, for example, a diffraction microrelief on large-format substrates is to obtain a technologically clean surface with homogeneously and uniformly distributed properties. This calls for higher requirements for cleaning various contaminants off substrate surfaces [66,108,162–165].

Existing technology for obtaining technologically clean surfaces offers techniques for rough and final cleaning. Rough cleaning serves to remove primary macrocontaminants and uses chemical etching with acids, alkalis, and solutions. But even after a substrate has been thoroughly rinsed in running distilled or deionized water, its surface will invariably be contaminated with the residual etching reagent. To remove this type of contamination, final-cleaning techniques are used that involve the use of highly pure chemicals or surface bombardment with low-temperature plasma particles. Final cleaning has a decisive effect on mask adhesion and takes place immediately before a mask is deposited on the substrate surface.

This section discusses the existing final-cleaning techniques widely used in diffractive optics and microelectronics.

### 3.1.1 Chemical Cleaning

Chemical cleaning consists of removing various types of contaminants from substrate surfaces through various methods: immersion in a washing solution or the saturated vapor of a liquid; boiling; ultrasonic treatment with complexones and surface-active agents (SAAs); hydromechanical treatment; rinsing in distilled and deionized water; and so on [109,166–175]. All these methods involve using many highly pure chemicals [168,174], process tooling made of chemically resistant materials, and various energy sources. This significantly complicates the environmental conditions of techniques used.

An example of the complexity inherent in chemical cleaning is the Lada-150 wafer-cleaning line comprising up to 10 process modules. Substrate treatment in such equipment takes place in a nitrogen-filled closed manufacturing system in which wafers are not exposed to the air [172]. Highly toxic chemicals such as $H_2SO_4 + H_2O_2$, $NH_4OH + H_2O_2 + H_2O$, $HF + H_2O$, $HCl + H_2O_2 + H_2O$, and $Na_2Cr_2O_7 + H_2SO_4 + H_2O$ solutions [174,175] are used as processing media. The trend to use SAAs to reduce toxicity does not solve the problem in its entirety since any chemical in large quantities is a source of environmental pollution—primarily, waste water pollution [109]. And since chemical-cleaning process flows are, as a rule, designed for specific types of substrates and contaminants, the entire process flow has to be reworked each time a parameter is changed. This accounts for the large number of works on new methods and techniques for chemical cleaning of substrate surfaces [164–173,175,176].

Thus, the chemical cleaning techniques have the following drawbacks:

- Necessity of using highly pure chemical reagents.
- High toxicity affecting the operability of equipment and requiring special measures to dispose of waste to reduce environmental pollution.
- Necessity of selecting an appropriate solvent (acid, alkali, SAA) for each type of contaminant.
- A broad range of process equipment and tooling (degreasing equipment, ultrasonic baths, vibrating centrifuges, drying ovens, exhaust hoods, etc.)
- Surface contamination with both residual reagents and the impurities contained in them [109].

But in the absence of versatile, efficient final-cleaning techniques, chemical techniques continue to be widely used in diffractive optics and microelectronics [109,128].

### 3.1.2 Laser Cleaning

Laser cleaning relates to "dry" treatment methods and consists of removing various types of contaminants from the surface by heating surface contaminants to a temperature sufficient for thermal desorption. The radiation intensity required to remove a given type of contaminant is selected from the range $P \approx 10^3$–$10^4$ W/cm$^2$—that is, the intensity values are relatively low. Surface contaminants are removable by using the surface-melting method. Even with the radiation intensity increased to $10^4$–$10^5$ W/cm$^2$, the method does not destroy the substrate material. But when the liquid-phase crystallization of the surface melt takes place, impurity atoms may spread into the depth of the molten layer, thereby adversely affecting the substrate properties. Impurity atoms are observed in the composition of surface contaminants and in the working chamber's atmosphere and spread according to their segregation coefficient.

A major drawback of laser cleaning is that radiation intensity is highly nonuniform across the beam [109,177–179]. This drawback results in nonuniform surface cleaning when an automated substrate-scanning system is used and in the possibility of mechanical stress occurring on the substrate surface that may cause the microrelief to deform during subsequent etching.

Because of the broad range of substrate materials used, surface cleaning requires the use of different lasers with a wavelength ranging from the mid-infrared to the deep ultraviolet. References 109, 178, and 179 discuss industrial laser-beam generators: $CO_2$ and CO lasers, yttrium-aluminum-garnet ($Y_3Al_5O_{12}$) lasers, ruby ($Al_{2-x}Cr_xO_3$) lasers, ultraviolet exciplex lasers, and copper vapor lasers. But none of these lasers is yet capable of efficiently cleaning all types of substrates [109,180]. As a result, many works have been devoted to modifying laser systems and methods for their use [109,177–180] in order to obtain technologically clean surfaces.

To summarize, laser technology for surface cleaning has the following drawbacks:

- Nonuniform cleaning and the necessity of using scanning systems that make the equipment more complex and increase its cost
- Surface-layer defects such as craters and wavelike relief

Because of these drawbacks, lasers are suitable only for highly specialized applications.

### 3.1.3 Low-Temperature Plasma Cleaning

Cleaning of substrate surfaces with low-temperature plasma takes place under vacuum conditions before film coatings are applied [181–186]. In this case, cleaning efficiency depends on the type of discharge used, the gas-discharge device's design features, and substrate size. For instance, when a substrate is cleaned with a

glow discharge, the substrate is placed on the anode's working surface. As a result, the gas-discharge device's parameters become dependent on the surface area being treated—that is, a loading effect [109,128,187] occurs.

Cleaning of large surface areas with magnetron-discharge plasma requires scanning the surface, because the charged particle flux generated by this discharge is nonuniform in its cross section. And in this case the surface is generally cleaned with either positive Ar ions (i.e., inert particles) or O ions. Because both processes involve physical sputtering [188], an increase in the efficiency of surface cleaning entails increasing the charged particles' energy, and this deteriorates the surface properties [109,128].

A major drawback with HF and SHF discharges is the loading effect, which is observed as a change in the density of the particles colliding with the surface in response to a change in the number of substrates or their surface areas. To stabilize gas-discharge parameters, optimal resonant frequency, power, gas inleakage rate, and other parameters must be determined. For instance, in the case of modern equipment that uses transformer-coupled plasma and capacitively coupled plasma, the presence of a drawing potential necessitates increasing the dimensions of the plasma-forming device by several times for larger substrates [184–186].

Another drawback with HF and SHF discharges is that their relatively high power (300–600 W) causes the surface properties of substrates to deteriorate [184–186,189]. To limit the deterioration, chemically active gases and gas mixtures are used that determine cleaning efficiency. Gases used must yield a large number of reactive particles that form volatile compounds with surface atoms, be nontoxic and nonexplosive in the gas phase and the gas-vapor phase, and noncorrosive. And the gases must not contaminate intrachamber components and evacuation lines or have a highly adverse effect on vacuum-pump parts and oil if vacuum pumps are used.

The most common techniques for low-temperature plasma cleaning involve using highly pure gases and gas mixtures ($H_2$, $O_2 + Ar + H_2 + N_2 + He$, $C_xF_y$, $CF_4 + O_2$, $Cl_2$, HCl, $NF_3$, $SF_4$, etc.). This significantly increases the cost of fabricating microelectronic and diffractive optical elements [34,35,109,128,162,177,181–185,187,189–194]. Abandoning the expensive gas techniques in favor of in-the-air cleaning would have a significantly beneficial economic effect.

Thus, surface cleaning with a low-temperature plasma flux generated with the devices outlined above has serious drawbacks whose elimination complicates the equipment, tooling, and operating conditions.

## 3.2 FORMATION MECHANISMS OF SURFACE PROPERTIES

As the properties of a substrate surface depend on the concentration of atoms and molecules adsorbed at the surface, surfaces can be classified into two categories: atomically clean surfaces and technologically clean surfaces.

An atomically clean surface is a surface that is free from foreign atoms and that is obtained under ultrahigh vacuum conditions through ion bombardment, high-temperature annealing, monocrystal cleaving, and other techniques [109,128,190]. For an atomically clean surface, the microrelief etch rate does

not vary across the entire mask–substrate interface, and etching does not distort microstructure shapes.

A technologically clean surface is a surface with certain physicochemical properties that contains adsorbate atoms in a quantity that affects neither the operating characteristics of the component being fabricated on that surface nor any subsequent processing.

Analyzing the composition of surface contaminants allows the contaminants to be classified into three categories:

1. Contaminants adsorbed at the surface from the environment
2. Contaminants from contact with process tooling, such as residual acids, alkalis, solutions, and other process materials
3. Contaminants adsorbed at the surface directly in the working chamber before etching, such as organic molecules' atoms present even in the high-vacuum environment of a dry-pumping system or vacuum-oil vapors from the forevacuum system in UVN vacuum setups [130,187,195]

Some atoms and molecules in categories 1 and 2 are capable of chemisorption—that is, of generating strong bonds at the surface. Currently, there are well-developed dry and wet etching techniques for removing contaminants [16,17,109,128,190,191,193,196–198]. For example, a standard chemical washing technique will remove most surface contaminants.

During final cleaning, removing some atoms and molecules in category 2 requires using expensive plasma-chemical equipment [16,17,34,35,187,199,200].

Category 3 contaminants are hardest to remove: they form at the substrate surface as separate atoms or monomolecular layers directly during the evacuation of the working chamber. In terms of how difficult contaminants are to remove, of the greatest interest is the UVN-2M-1 vacuum evaporator, which incorporates oil-diffusion and forevacuum pumps and which is widely used in the microelectronic industry. Process-liquid vapors constitute the primary contamination source. When a mineral oil is used (such as VM-1), their flows reach the level of 0.5 μg/h · cm$^2$ [130,187]. That is why, for purposes of this monograph, VM-1 vacuum oil, whose properties are well known, was used as an organic-contaminant simulator. To determine the mechanism of how molecules are distributed in such flows during the evacuation of the working chamber, the test substrates were placed on a substrate carousel (positions I, II, III, and IV in Figure 3.1).

The adsorption rate of vacuum-oil molecules at the substrate surfaces was controlled by changing the time of evacuation with a mechanical pump (to a pressure of 3.5 Pa) and a diffusion pump (to a pressure of $3.99 \cdot 10^{-3}$ Pa). Figure 3.2 shows the results of the experiments. Surface cleanliness was measured with the technique presented in Reference 70.

As curves 1, 2, 3, and 4 show, the substrates with chemically cleaned surfaces are characterized by a significantly increased degree of contamination in the ranges $T < 5$ min (curves 1 and 2), $T < 5.4$ min (curve 3), and $T < 7$ min (curve 4). The increase is presumably due to adsorption of atmospheric hydrocarbons present in the vacuum chamber and of vacuum-oil molecules brought by their backflow from

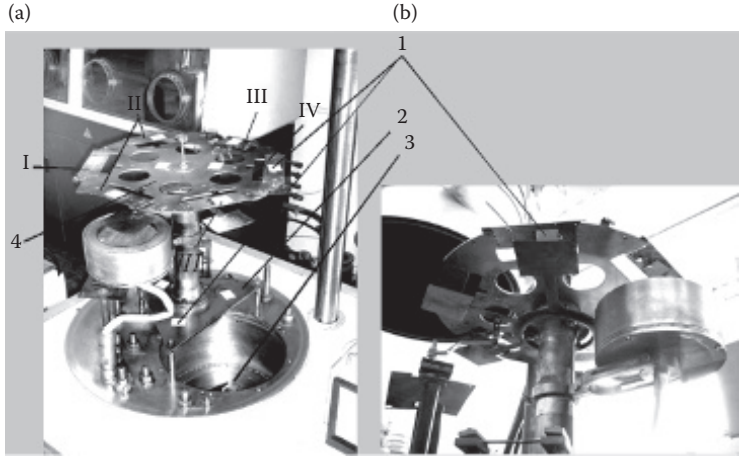


**FIGURE 3.1** Arrangement of substrates in UVN-2M-1's working chamber: (a) top view and (b) bottom view. (1) Test substrate, (2) carousel base, (3) diffusion-pump valve, and (4) substrate carousel.

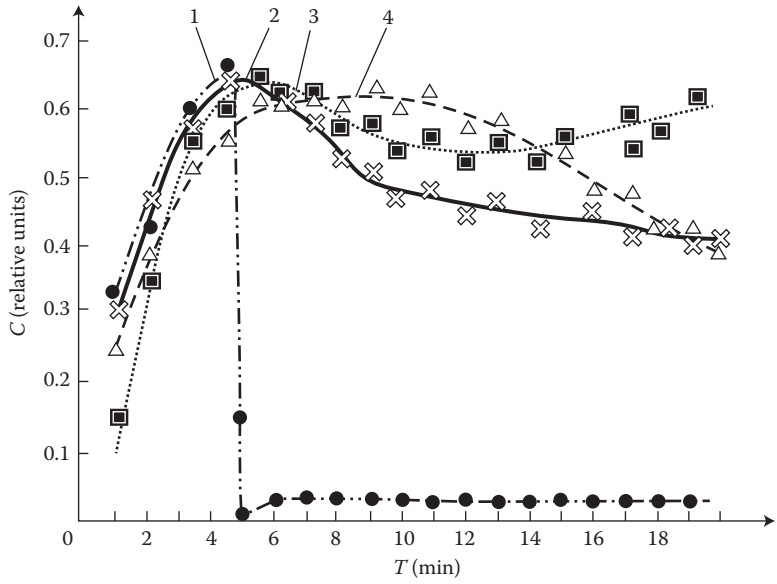


**FIGURE 3.2** Curves characterizing the degree of surface contamination with vacuum-oil molecules: (1) curve characterizing surface cleanliness before ($T \leq 5$ min) and after ($T > 5$ min) final cleaning and (1)–(4) substrate contamination for different substrate positions on the carousel.

the mechanical and diffusion pumps. The drop of curves 2, 3, and 4 outside the ranges indicates desorption of these molecules from the surface.

As the flows of vacuum-oil molecules from the evacuation system are nonuniform, the degree of their effect on substrate contamination differs depending on the position of a given substrate on the carousel (positions I, II, III, and IV in Figure 3.1). For instance, during the 2-h evacuation period, the substrates placed on the carousel base (2)—that is, those in a region outside the direct impact of the oil backflow—were contaminated 1.6 times less than those placed on the carousel surface.

From this it follows that the primary contaminant in UVN-2M-1's working chamber is vacuum oil, a product used in its evacuation system.

The substrates in position II on the carousel, on reaching a contamination level corresponding to $T = 5$ min, were bombarded with off-electrode plasma particles at a discharge current of $I = 10$ mA and an electrode voltage of $U = 1.2$ kV for a period of $t = 10$ s (see curve 1 in Figure 3.2). The manner in which curve 1 changes shows that bombardment with plasma particles efficiently cleans vacuum-oil molecules off the substrate surface. At $T > 5$ min, the surface contamination increases slightly by no more than 3%.

With these results in mind, we conclude that:

1. Contamination of substrate surfaces in the vacuum system's working chamber is a function of how the backflow of vacuum oil from the vacuum-pump system is distributed.
2. Primary contamination takes place within the first five minutes of evacuation with a mechanical pump; then the atoms and molecules of organic contaminants are desorbed.
3. Efficient cleaning must take place as part of forming a forevacuum at $T \geq 5$ min.

## 3.3 MOLECULAR STRUCTURE ANALYSIS OF THE ORGANIC CONTAMINANT

A characteristic feature of the vacuum-oil molecule is its spatial arrangement on the substrate surface (see Figure 3.3) [201,202].

As the bond angles in the six-membered ring are equal to the normal valence angle of carbon (109° 28′), the bonds do not deviate from their normal direction and

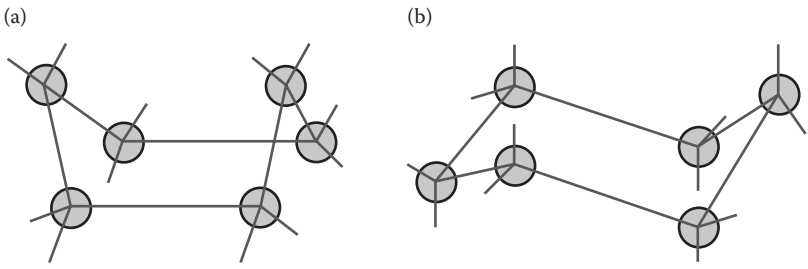


**FIGURE 3.3** Carbon skeletons of cyclohexyl: (a) tub shape and (b) armchair shape.

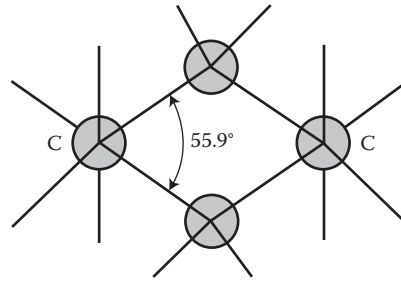


**FIGURE 3.4** Carbon skeleton of cyclohexyl.

the cyclohexyl ring is highly stable. As a rule, cyclohexyl bonds have an armchair shape because the atomic binding energy in this molecule is less than that in a molecule with a tub-shaped carbon skeleton [201]. The cross section of the armchair-shaped cyclohexyl molecule is characterized by large height dimensions (Figure 3.4).

Consider the spatial arrangement of carbon and hydrogen atoms in the oil molecule whose main component is $C_{33}H_{64}$ [201]. For purposes of this discussion, we will divide this molecule into three characteristic parts (see Figure 3.5): $C_6H_{11}$–; $-(CH_2)_{25}-$; and $-CH = CH_2$. In the first part, the arrangement of carbon atoms and hydrogen atoms corresponds to that in the ethylene molecule [202], except that one hydrogen atom is replaced with a carbon atom (see Figure 3.5). The second part is a long side chain consisting of $CH_2$ atom groups.

Adsorption of oil molecules at substrate surfaces is determined by Van der Waals forces [99], and the resultant bond is comparatively weak. For instance, the heat of physical adsorption of vacuum-oil vapors on carbon is $90–100 \cdot 10^6$ J/kmol [201]. Depending on whether the adsorbed molecule and the adsorbent have polar properties, the following characteristic types of interaction can occur during physical adsorption [203]:

- Adsorption of nonpolar molecules ($H_2$, $O_2$, $N_2$, etc.) on a nonpolar adsorbent (solids with atomic and molecular lattices such as graphite, diamond, and organic-substance crystals).
- Adsorption of nonpolar molecules on a polar adsorbent (solids with ionic lattices).
- Adsorption of polar molecules on a nonpolar adsorbent.

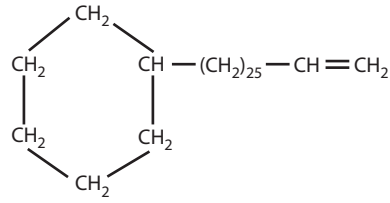


**FIGURE 3.5** Structural formula of the vacuum-oil molecule.

The interaction mechanism of polar molecules and polar adsorbents is similar to the mechanism whereby a polar adsorbent adsorbs a nonpolar molecule [203]. Because vacuum oils are based on the component $C_{33}H_{64}$, all hydrocarbons are nonpolar [201]. Therefore, the usual dispersion forces are supplemented by induction forces—the positive and negative ions of the solid's lattice that induce opposite-sign charges in a nonpolar molecule. This results in an additional electrostatic attraction of the adsorbed molecule by the polar adsorbent.

According to Reference 187, the binding energy between the oil-molecule atoms and the substrate atoms is greater than that between the oil-molecule atoms; we can suppose that even when oil molecules are effectively desorbed from the substrate surface, a monomolecular contaminant layer will invariably be present on it [109,187] and that the layer's thickness depends on the atoms' structural arrangement (see Figure 3.6).

The thickness of the oil-molecule layer can be derived from the expression

$$h_f = h_K + 2 \cdot h'_{CH} + \frac{h_H}{2} + h_{ad}, \tag{3.1}$$

where $h_f$ is the film thickness (nm); $h_K$ is the distance between opposite carbon atoms in the $C_6H_{11}$ ring (nm); $h'_{CH}$ is the projection of the C–H bond's length on the axis perpendicular to the substrate surface (nm); $h_H$ is the orbital radius of the hydrogen atom (nm); and $h_{ad}$ is the distance determined by film–substrate adhesion (nm).

The molecule structure in Figure 3.6a yields the following equation:

$$h_K = h_{CC} + 2 \cdot h_{CC} \cdot \sin\left(90 - \frac{\alpha}{2}\right), \tag{3.2}$$

where $h_{CC}$ is the length of the C–C bond (nm).

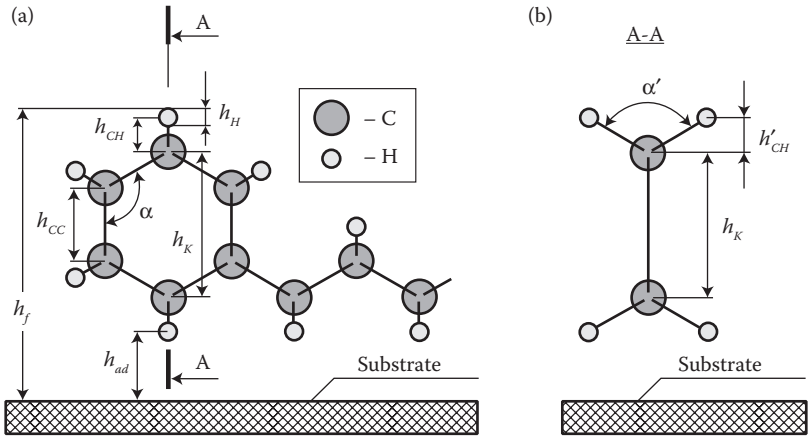


**FIGURE 3.6** Arrangement of an oil molecule on the substrate surface: (a) longitudinal cross section and (b) transverse cross section.

The value of $h_{CH}^{|}$ can be determined from the transverse cross section shown in Figure 3.6b:

$$h_{CH}^{|} = h_{CH} \cdot \cos\left(\frac{\alpha'}{2}\right), \tag{3.3}$$

where $h_{CH}$ is the length of the C–H bond (nm) and $\alpha'$ is the bond angle of $CH_2$ atoms.

It is known that $h_H = 0.05$ nm [202], $h_{CH} = 0.109$ nm, $h_{CC} = 0.154$ nm [202], and $h_{ad} = 0.5$ nm [203]. Substituting the numerical values into Equations 3.1 through 3.3 gives

$$h_f = 0.154 + 2 \cdot 0.154 \cdot \sin\left(90 - \frac{109.47}{2}\right)$$
$$+ 2 \cdot 0.109 \times \cos(58.35) + \frac{0.05}{2} + 0.5 = 0.974\,\text{nm}.$$

Because the $h_f$ obtained from this method agrees well with the data presented in Reference 187, we will assume, for purposes of further discussion, that the thickness of the oil film on the substrate surface equals $h_f \approx 1$ nm.

Thus, during evacuation, a hard-to-remove monomolecular layer of vacuum-oil molecules forms on substrate surfaces.

## 3.4 PREPARING INITIAL SAMPLES WITH A GIVEN DEGREE OF CONTAMINATION

The investigation was carried out on $30 \times 20 \times 1$ mm polycrystalline and silicon dioxide ($SiO_2$) substrates because these two types are the most widely used in fabricating various DOEs and nano- and microelectronic elements.

There are several methods for depositing monomolecular films of organic contaminants on the substrate surface: immersing substrates in a vacuum-oil solution and then in toluene or dichloroethane, followed by drying [18]; centrifuging a vacuum-oil solution; and spreading an oil drop on a water surface (the Langmuir–Blodgett method) [204,205]. But these methods do not allow a film structure to be formed whose qualitative composition would be identical to that of contaminants formed on a substrate in the vacuum chamber, because the solvents act as contaminants themselves and solvent molecules will be present at the substrate surface along with vacuum-oil molecules.

Further, vacuum-oil molecules are polydisperse—that is, each of them can have different molecular weights. This causes the film to be nonuniformly distributed on the substrate surface when the methods of immersion and centrifuging are used. The Langmuir–Blodgett method is also inapplicable: it gives densely compressed film structures that do not match those of films formed in the vacuum chamber.

To overcome these shortcomings, this section proposes using the vacuum evaporation method involving the use of the surface contaminator shown in Figure 3.7 for depositing monomolecular films whose properties and structure match those of substrate contaminants formed in the vacuum chamber.

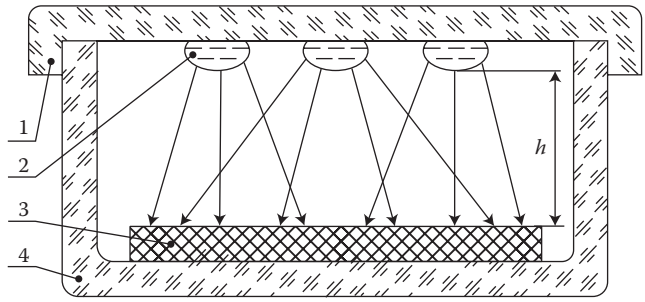


**FIGURE 3.7** Design of the surface contaminator [136]: (1) quartz-vessel lid, (2) drops of VM-1 vacuum oil, (3) substrate, and (4) quartz vessel.

The contaminator is a closed quartz vessel. A substrate is placed into the quartz vessel, and then vacuum-oil drops (a source of organic contaminants whose properties are well known) are deposited on the lid's inner surface. The quartz vessel is covered with the lid and placed into UVN-2M-1's working chamber, which is then evacuated to a pressure of 1.33 Pa at a temperature of 300 K.

Under these conditions, the mean free path of evaporating oil molecules equals the distance between the drops' surfaces and the test substrate (≈5 mm). Because oil molecules reach the substrate surface without interacting with other compounds' molecules in the vacuum chamber, the contaminants adsorbed at the surface show uniform properties. Each contamination regime was reproduced at least 10 times, with the parameter spread no greater than 10%.

The initial substrates' surfaces had a large amount of contamination (see Figure 3.8a) whose numerical value, $C_d$, was measured in relative units with the technique described in References 70 and 71.

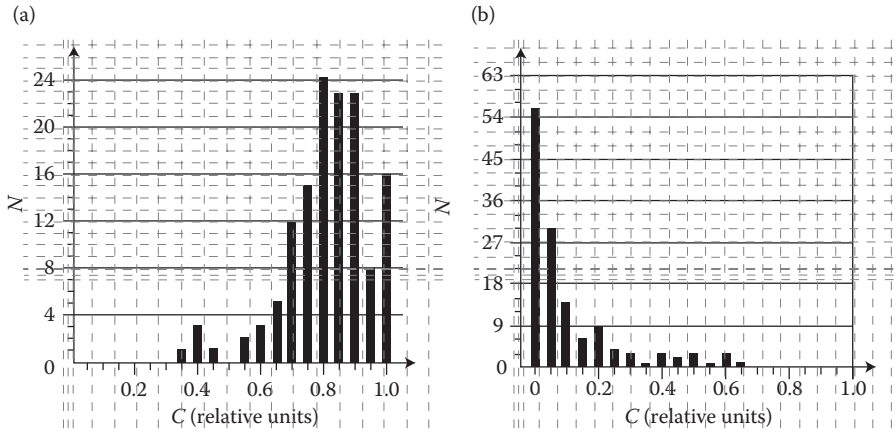


**FIGURE 3.8** Graphs showing substrate distribution by degree of initial surface contamination: (a) contamination degree of initial substrates and (b) contamination degree of chemically cleaned substrates.

As the bars in Figure 3.8a show, 69% of the substrates (94 substrates out of 136) showed a contamination level greater than 0.8 relative units ($0.802 \cdot 10^{-7}$ g/cm$^2$). To remove this contamination, the substrates were roughly cleaned by chemical etching through the technique whose steps are outlined below:

1. Rubbing with a cambric cloth soaked in ethyl alcohol on both sides, to remove large mechanical particles
2. Boiling in distilled water for 10 min
3. Boiling in an alkali solution for 10–15 min
4. Boiling in distilled water for 10 min
5. Boiling in ethyl alcohol for 10 min

This cleaning removed the greater part of contaminants with unknown parameters (see Figure 3.8b) from the substrate surfaces. But some substrates still showed a contamination level up to 0.65 relative units. This indicated the presence of hard-to-remove, chemically bonded contaminants formed at the time the substrates were made and removable only with special chemical or plasma-chemical cleaning techniques. As a result, all chemically cleaned substrates used in the experiment were screened to reduce the spread of cleanliness values to 0.03%. Then the substrates were placed on the bottom of the quartz vessel.

The concentration of contaminants at the test surface was controlled by changing the time ($t$) that the substrates were held in the contaminator inside the vacuum chamber. The value of $t$ varied from 0 to 90 min. At $t = 60$ min and a chamber pressure of 1.33 Pa, the pulse time $\tau$, which characterizes the degree of surface cleanliness, reduced to $0.05 \cdot 10^{-2}$ s (see Figure 3.9) and remained unchanged in the range $60 \le t \le 90$ min because of the saturated contamination process and the stabilized friction coefficient, which, according to Reference 109, are achieved when the concentration of organic contaminants at the surface reaches $10^{-7}$–$5 \cdot 10^{-6}$ g/cm$^2$.

An examination with an atomic force microscope confirmed that a film of vacuum oil forms on substrate surfaces subjected to contamination for a period of $t = 60$ min (see Figure 3.10).

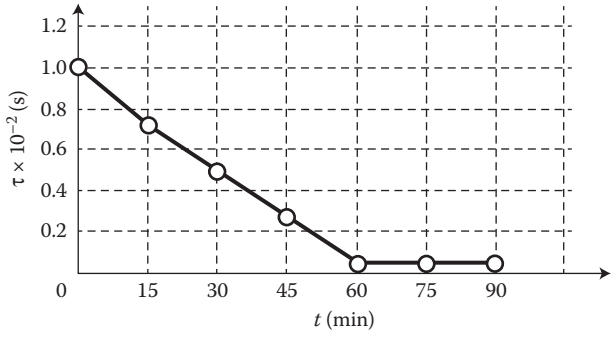


**FIGURE 3.9** Relationship between the degree of contamination of substrate surfaces and the time that the substrates are held in the contaminator inside the vacuum chamber: $\alpha = 45°$ and $\beta = 5.5°$.

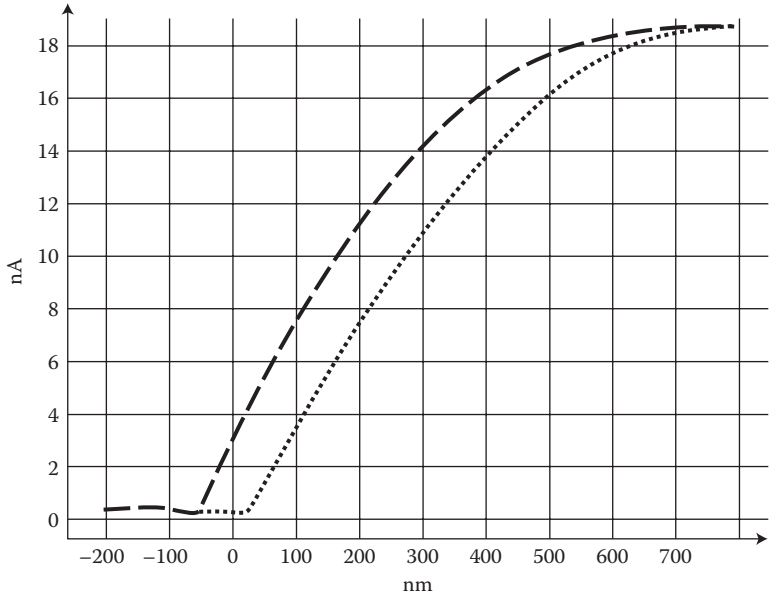


**FIGURE 3.10** Force curve obtained with Solver PRO-M for the test surface before final cleaning. The interaction distance between the cantilever and the surface structure is a 3-nm film of organic contamination.

According to the calculations presented in Section 3.3, a 3-nm-thick film should comprise three layers of vacuum-oil molecules, but as reported in References 206–208, in examinations with an atomic force microscope, the molecular layer wets the cantilever, thereby causing hysteresis in measurements and increasing the related readings. When monomolecular films are measured with contact atomic force microscopy, vacuum-oil molecules may elongate and become polarized, which is an effect that determines the 3 nm thickness and agrees with the calculated molecule length. Calculating the height of the molecule (see Figure 3.6) turned to a vertical position yields a value of 3.41 nm. This signifies that the scanning probe microscope indeed measures the monomolecular layer of vacuum oil.

Thus, the initial sample surfaces were obtained by storing the substrates in the quartz vessel for 60 min at a pressure of 1.33 Pa and a temperature of 300 K after final cleaning. After some of the substrates were ruled out, the reproducibility of forming a monomolecular layer of organic contaminants on an initial substrate surface amounted to 99.5%.

## 3.5 ANALYSIS OF PLASMA PARTICLES IMPINGING ON THE SURFACE BEING TREATED

This monograph discusses treating surface materials with low-temperature plasma generated by a high-voltage gas discharge outside the electrode gap in a nonuniform electric field in which negatively charged particle fluxes (negative ions and electrons)

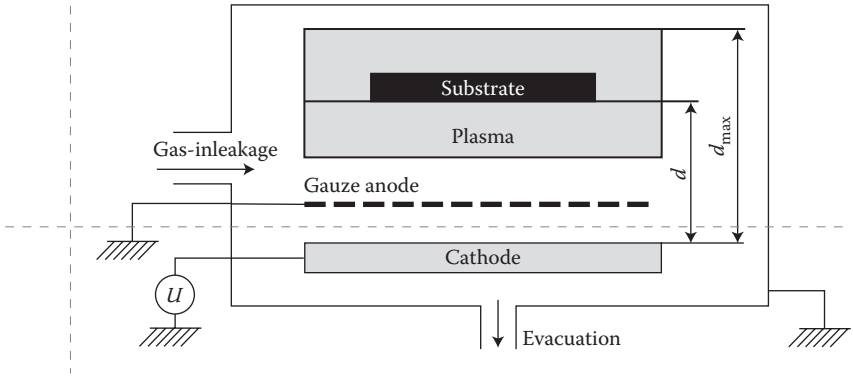


**FIGURE 3.11** Schematic of the reactor.

are generated that are incident on the surface being treated. Figure 3.11 shows the schematic of the reactor used for this purpose.

To determine what interaction mechanisms take place between plasma particles and the surface, we will briefly analyze the processes that occur in high-voltage gas-discharge plasma. It is known that the progress of a process occurring in gas-discharge plasma depends on the mean free path and the number of collisions, as well as on the particle energy. The particle energy is, in turn, determined by the gradient of voltages applied to the electrodes of the gas-discharge device, whose action in a nonuniform electric field is a function of distance. This relationship is presented in Reference 65 as

$$y = \frac{hU_n}{U} + 2c\,tg\left(\frac{\pi U_n}{2U}\right), \tag{3.4}$$

where $U_n$ is the electric-field potential at a distance of $y$ from the cathode (V). For purposes of calculating $U_n$ outside the electrodes, we can disregard the first term in Equation 3.4 (because it is small as compared with the second one) and express $U_n$ as follows:

$$U_n = \frac{2U}{\pi}\text{arc}\,tg\left(\frac{y}{2c}\right). \tag{3.5}$$

Now if we assume that $y$ is the mean free path of the charged particle ($\lambda$) multiplied by the number of its collision ($n$) and substitute this product into Equation 3.5, then $U_n$ will represent the potential difference passed through by the particle after each collision. Then the accelerating potential difference after each collision can be described by

$$\Delta U_n = U - \frac{2U}{\pi}\text{arc}\,tg\left(\frac{n\lambda}{2c}\right) = U\left(1 - \frac{2}{\pi}\text{arc}\,tg\left(\frac{n\lambda}{2c}\right)\right). \tag{3.6}$$

Taking into account the energy lost by the particle in collision with process-gas molecules, the particle's full energy after each collision is given by

$$E_n = E_{n-1}(1-\gamma) + e\Delta U_n, \tag{3.7}$$

where $\gamma = 4mM/(m+M)^2$; $m$ is the weight of a charged particle and $M$ is the weight of a process-gas molecule.

Note that $n$ varies from one to the number of collisions that the particle has time to undergo in covering the distance from the cathode to the sample surface ($d = 4.5$ cm in the case under study). With expression (3.5), it is also possible to calculate the maximum distance over which the ion-plasma flux propagates at a given electrode voltage. Assuming that $U_n = U - U_1$, where $U_1$ is a penalty function (obtained from a natural experiment) and a constant equal to $U_1 = 1$ V, we obtain the following expression:

$$d_{\max} = 2c\ tg\left[\frac{\pi}{2}\left(\frac{U-U_1}{U}\right)\right], \tag{3.8}$$

where $d_{\max}$ is the maximum distance over which the ion-plasma flux propagates. Expression (3.8) is valid because as the accelerating voltage increases, the distance $d_{\max}$ increases as well (this relationship was visually observed during the experiment). Therefore, an essential condition to starting a treatment with high-voltage gas-discharge off-electrode plasma is

$$d_{\max} > d. \tag{3.9}$$

Simultaneous analysis of expressions (3.6) and (3.7) shows that in the case of a large number of collisions and a small free path (conditions typically observed at low electrode voltages on the order of the ignition voltage), $E_n$ falls within the energy range typical of plasma-chemical etching (see Figure 3.12). From the graph in Figure 3.12 it follows that as the voltage increases, $E_n$ increases too. At a certain electrode voltage, $E_n$ is sufficient for physical sputtering as well (ion-plasma etching). And if the charged particles are chemically active toward the material being treated, material removal due to chemical reactions occurs along with sputtering—that is, ion-chemical etching takes place.

According to the law of distribution of equipotential lines (see Figure 1.2), the accelerating voltage reduces in the direction of $d_{\max}$ at a given fixed voltage at the gas-discharge device's electrodes. This means that by moving the sample from the cathode along the discharge direction, one can change the accelerating voltage in the treatment area. To think of it another way, if a given voltage is applied to the electrodes that exceeds the ignition voltage of high-voltage gas discharge and if the sample is moved along the plasma flux, one can always determine the areas of ion-chemical etching and plasma-chemical etching as well as the transition area (see Figure 3.13), whose etching mechanism will be discussed below.

Let us consider what particles will collide with the surface being treated in each of these areas, assuming by way of illustration that fluorinated gas is used as plasma-forming gas.

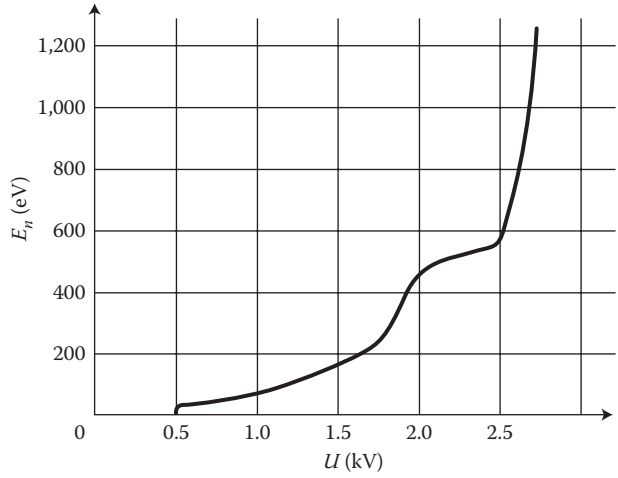


**FIGURE 3.12** Relationship between the energy of negative ions bombarding the sample and the electrode voltage at a discharge current of $I = 140$ mA.

In the plasma-chemical etching area, the following particles contribute to the process:

- Negative $F^-$ ions (flux $J_i^-$) generated in plasma as a result of electron attachment to the neutral fluorine atoms [92] under whose action chemically active particles (CAPs) are desorbed from the surface being treated (the desorption is characterized by the desorption coefficient $k_2$) and material etching takes place (the etching is characterized by the coefficient $k_1$).
- Chemically active neutral fluorine radicals (CAPs in the flux $J_a$), which can form reaction products that are volatile at the process temperature when colliding with the atoms of the material being treated. (Only those negatively charged particles move toward the surface that are not passive toward the material being treated [62].)
- Passivating particles (flux $J_p$). (Their flux incident on the surface is negligible because the surface being treated is outside the discharge-generating

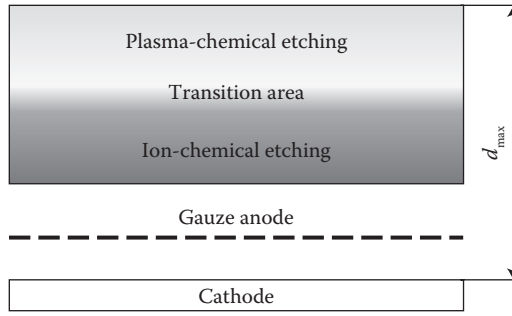


**FIGURE 3.13** Arrangement of etching areas in high-voltage gas-discharge plasma.

electrodes, which in itself excludes the generation of passivating particles as a result of cathode sputtering and therefore their effect on etching in general.)

- Neutral molecules of fluorinated gas (flux $J_n$), whose dissociation under the action of ion bombardment results in chemically active fluorine radicals forming at the surface.

In the ion-chemical etching area, only negative $F^-$ ions (flux $J_i^-$) will impinge on the surface during etching. In addition to physical sputtering characterized by the sputtering coefficient $k_3$, these ions will also etch the material because of the chemical reaction taking place. Given the heating of the material by high-energy $F^-$ ions, which reduces the number of collisions between CAPs and the surface because of desorption, we can disregard the effect that CAPs have on etching in this area.

## 3.6 MECHANISM OF SURFACE CLEANING WITH DIRECTED FLUXES OF LOW-TEMPERATURE OFF-ELECTRODE PLASMA

### 3.6.1 Cleaning Mechanism

The substrate surfaces were cleaned with high-voltage gas-discharge plasma. As noted earlier, in this plasma, only negatively charged particles move toward the surface. When the process gas is air containing 78% nitrogen and 21% oxygen, the particles will be represented by negative oxygen ions and electrons. Positive nitrogen and oxygen ions will move toward the gas-discharge device's cathode.

At high gas pressures in the working chamber (i.e., at low accelerating voltages in the range $0.5 \le U \le 1$ kV), the substrate surface will invariably have an adsorbed layer of neutral molecules of NO, $N_2O$, and $NO_2$, which result from the recombination of oxygen ions and nitrogen ions [66], and of $N_2$ and $O_2$ molecules. Without additional activation, chemical reactions of these compounds with the molecules of organic contaminants (hydrocarbons $-C_xH_y-C_mH_n-$) either do not take place or are weak.

With ion bombardment, contaminants are removable with the technique for plasma-chemical etching described in detail in References 209 and 210 and in Chapter 5. Under the action of ion bombardment, the neutral molecules of NO, $N_2O$, $NO_2$, $N_2$, and $O_2$ dissociate at the surface to form positive nitrogen and oxygen ions, which begin to move along the electric-field lines toward the cathode, and oxygen radicals, which actively interact with free surface hydrocarbon bonds. The oxidation of organic contaminants occurs in a chain of reactions, apparently in the following steps [190]:

$$\mathrm{RH + O \rightarrow \dot{R} + \dot{O}H;} \quad \mathrm{R\dot{O}O + RH \rightarrow ROOH + \dot{R};}$$
$$\mathrm{RH + O \rightarrow \dot{R}' + \dot{R}''O;} \quad \mathrm{ROOH \rightarrow \dot{R}O + \dot{O}H;}$$
$$\mathrm{RH + \dot{O}H \rightarrow \dot{R} + H_2O;} \quad \mathrm{\dot{R}_nO \rightarrow R_{n-1}O' + RO;}$$
$$\mathrm{\dot{R} + O_2 \rightarrow ROO';} \quad \mathrm{2\dot{R} \rightarrow R_2,}$$

where R and $\dot{R}$ are the fragments and radicals of organic-contaminant molecules and R′ and R″ are radicals derived from R and formed during the breakdown of contaminant molecules. As a result of such reactions, the film of organic contaminants is broken down into individual fragments that have a low-molecular mass, and then the fragments are oxidized, yielding CO and $CO_2$, as well as $H_2O$ vapor.

At an accelerating voltage of $U > 1$ kV, the removal of organic contaminants will occur under the mechanism of ion-chemical etching described in detail in References 209 and 210, and in Chapter 5. But as can be seen from Figure 3.14, at an irradiation time of up to 50 s, a discharge current of up to 10 mA, and an accelerating voltage of up to 3 kV, the substrate temperature does not exceed 360 K [211]. Therefore, adsorption of neutral molecules at the surface is possible, and the ion-chemical etching mechanism of contaminants differs from the mechanism discussed earlier in that the neutral molecules of NO, $N_2O$, $NO_2$, $N_2$, and $O_2$ are present at the surface that serve as sources for the formation of chemically active oxygen radicals. From this it follows that contaminants will be removed not only by the ion-chemical etching described in References 209 and 210 but also by the mechanisms of ion-stimulated etching and electron-stimulated radical etching [212,213].

Contaminant removal comprises the following key processes:

1. Physical sputtering with negative oxygen ions
2. Chemical etching with negative oxygen ions
3. Chemical etching with oxygen radicals formed through the dissociation of neutral molecules as a result of bombardment with negative oxygen ions

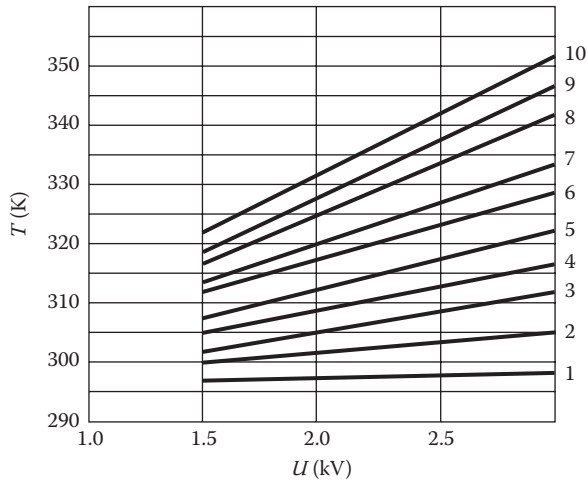


**FIGURE 3.14** Experimental relationship between substrate temperature and accelerating voltage: (1) $I = 1$ mA, (2) $I = 2$ mA, (3) $I = 3$ mA, (4) $I = 4$ mA, (5) $I = 5$ mA, (6) $I = 6$ mA, (7) $I = 7$ mA, (8) $I = 8$ mA, (9) $I = 9$ mA, and (10) $I = 10$ mA. Irradiation time $t = 50$ s.

4. Chemical etching with oxygen radicals formed through the dissociation of neutral molecules as a result of electron impact

Physical sputtering of organic-contaminant particles causes unsaturated valence bonds to form that are highly chemically active and thus intensify the chemical reactions to a greater degree.

From References 190 and 214, it is known that hydrocarbons are capable of polymerization when exposed to a plasma flux. The polymerization rate is proportional to the process temperature [215]. As a result of polymerization, the molecules of organic contaminants merge into long, cross-linked chains. The strengthening of molecular bonds impedes the removal of organic-contaminant particles from the substrate surface and slows down the cleaning process. According to Reference 215, the most efficient polymerization occurs at a temperature equal to or greater than 400 K. But at a process temperature of 360 K or below, the polymerization rate does not exceed 0.96% per hour; therefore, for purposes of this monograph, polymerization is negligible. In this case, the total contaminant-removal rate depends on the rates of the processes discussed above.

### 3.6.2 Cleaning Model: Primary Expressions

We will determine surface cleanliness as the relationship between the variation value of the surface concentration of contaminants, the contaminant-removal rate ($V_{et}$), and the irradiation time ($t$):

$$C_d = C_{(0)d} - V_{et}\rho t, \tag{3.10}$$

where $C_{(0)d} = h \cdot \rho$ is the initial concentration of surface contaminants; $h$ is the thickness of the contaminant film; and $\rho$ is the contaminant density. We propose that $V_{et}$ be expressed as a sum of rates:

$$V_{et} = V_{ich} + V_{ist} + V_{est}, \tag{3.11}$$

where $V_{ich}$ is the ion-chemical etch rate; $V_{ist}$ is the ion-stimulated radical etch rate; and $V_{est}$ is the electron-stimulated radical etch rate. Considering the presence of neutral molecules at the surface, the ion-chemical etch rate is given by [209]

$$V_{ich} = \left(\frac{B(k_1 + k_3)M}{\rho N_A}\right)\left|\exp\left(\frac{U - U_{gd}}{U}\right) - 1\right| \times J_i^-(1-\theta), \tag{3.12}$$

where $B$ is the value of the penalty function obtained from a natural experiment (a constant); $k_1$ and $k_3$ are the coefficients of plasma-chemical etching and physical sputtering, respectively; $M$ is the molar mass of organic contaminants; $U_{gd}$ is the electrode voltage at which the ion energy lies at the boundary between the

energies of plasma-chemical etching and ion-chemical etching at the moment the ion approaches the surface being treated; $J_i^-$ is the flux of negative ions incident on the substrate; and θ is the degree of surface filling by active particles. The value of $J_i^-$ is given by [209]

$$J_i^- = \left(1 - \frac{d}{d_{\max}}\right) \frac{I}{qeS_K} \left(1 - \frac{\gamma_e\ \eta}{(1+\gamma_e)} \exp[(\alpha - \alpha_n) d_{\max}]\right), \tag{3.13}$$

where $(1 - d/d_{\max})$ is a multiplier that numerically characterizes those ions from the aggregate flux that reach the sample surface and that contribute to the etching, as long as $d_{\max} > d$, where $d_{\max}$ is the maximum distance over which the ion-plasma flux propagates, and $d$ is the distance to the substrate; $S_K$ is the cathode surface area; $q$ is the geometric transparency of the gauze anode; and $\gamma_e$, α, and $\alpha_n$ are the coefficients of secondary emission, ionization, and attachment, respectively. Dissociation of four molecule types—NO, $N_2O$, $NO_2$, and $O_2$—generates chemically active oxygen radicals at the surface. Therefore, the total degree of surface filling by active particles equals

$$\theta = \theta_{NO} + \theta_{N_2O} + \theta_{NO_2} + \theta_{O_2}. \tag{3.14}$$

If plasma does not contain passivating particles, $\theta_{NO}, \theta_{N_2O}, \theta_{NO_2}$, and $\theta_{O_2}$ can be expressed as

$$\begin{aligned} \theta_{NO} &= 1/\left[1 + \frac{(k_1 + k_2^{NO})\, J_i^-}{s_a\, J_n^{NO}}\right], \quad \theta_{NO_2} = 1/\left[1 + \frac{(k_1 + k_2^{NO_2})\, J_i^-}{s_a\, J_n^{NO_2}}\right], \\ \theta_{N_2O} &= 1/\left[1 + \frac{(k_1 + k_2^{N_2O})\, J_i^-}{s_a\, J_n^{N_2O}}\right], \quad \theta_{O_2} = 1/\left[1 + \frac{(k_1 + k_2^{O_2})\, J_i^-}{s_a\, J_n^{O_2}}\right], \end{aligned} \tag{3.15}$$

where $k_2^{NO}$, $k_2^{N_2O}$, $k_2^{NO_2}$, and $k_2^{O_2}$ are desorption coefficients for NO, $N_2O$, $NO_2$, and $O_2$ molecules calculated with the method presented in Reference 214:

$$k_2^i = \frac{3}{4\pi^2} \beta_i \frac{4mM_i}{(m + M_i)^2} \frac{E_n}{E_{sv}}, \tag{3.16}$$

where $\beta_i$ is a unitless parameter dependent on the mass ratio of the incident ion ($m$) and the target particle of the $i$ type of molecule ($M_i$); $E_n$ is the ion energy at the moment the ion approaches the surface; and $J_n^{NO}$, $J_n^{N_2O}$, $J_n^{NO_2}$, and $J_n^{O_2}$ are neutral-molecule fluxes incident on the substrate surface, and they are calculated with the methods presented in References 190 and 216. The aggregate coefficient of physical sputtering is given by

$$k_3 = k_3^C + k_3^H, \tag{3.17}$$

where $k_3^C$ and $k_3^H$ are the coefficients of physical sputtering derived from Equation 3.16 for carbon and hydrogen atoms, respectively.

Given these calculations, the ion-stimulated etch rate can be determined from [212]

$$V_{ist} = \frac{Bk_i^* k_1 M}{\rho N_A} J_i^- \theta, \tag{3.18}$$

where $k_i^*$ is the unitless coefficient of ion-stimulated etching. Similar to Equation 3.18, the electron-stimulated etch rate can be expressed as [213]

$$V_{est} = \frac{Bk_e^* k_1 M}{\rho N_A} J_e \theta, \tag{3.19}$$

where $k_e^*$ is the unitless coefficient of electron-stimulated etching and $J_e$ is the electron flux incident on the substrate surface, and it is derived from the following expression [209]:

$$J_e = \frac{I\gamma_e \eta}{eqS_K(1+\gamma_e)} \exp[(\alpha - \alpha_n)d_{\max}]. \tag{3.20}$$

By substituting Equation 3.17 into Equation 3.12 and Equations 3.12, 3.18, and 3.19 into Equation 3.11 and transforming the equations, we obtain the final expression for determining the aggregate removal rate for organic contaminants:

$$V_{et} = \frac{BM}{\rho N_A} \times \left[ (k_1 + k_3^C + k_3^H) \left| \exp\left( \frac{U - U_{gd}}{U} \right) - 1 \right| J_i^-(1-\theta) + k_i^* k_1 J_i^- \theta + k_e^* k_1 J_e \theta \right]. \tag{3.21}$$

Given Equations 3.11 and 3.21, the expression for determining the variation value of the surface concentration of organic contaminants can now be expressed as [217,218]

$$C_d = \rho h - \frac{BM}{N_A} \times \left[ (k_1 + k_3^C + k_3^H) \left| \exp\left( \frac{U - U_{gd}}{U} \right) - 1 \right| J_i^-(1-\theta) + k_i^* k_1 J_i^- \theta + k_e^* k_1 J_e \theta \right] t. \tag{3.22}$$

The proposed analytical relationship makes it possible to reduce the volume of expensive and complex research into the effect that the parameters of ion–electron

bombardment have on cleaning. The calculation results obtained with expression (3.22) can be directly used in technology for fabricating DOEs and nano- and microelectronic elements.

## 3.7 EXPERIMENTAL INVESTIGATION INTO THE RELATIONSHIP BETWEEN THE DEGREE OF SURFACE CLEANLINESS AND PHYSICAL PLASMA PARAMETERS

Experimental variation values of the surface concentration of organic contaminants were measured with the tribometric method based on the relationship between the probe's sliding speed on the test surface and the concentration of organic contaminants adsorbed at the surface [70] (for details, see Chapter 2).

Figures 3.15 through 3.17 show experimental graphs that represent the relationship between the surface concentration of organic contaminants on plasma-cleaned substrates and three process factors: accelerating voltage, irradiation time, and discharge current [181,219].

The curves in Figure 3.15 show that, depending on the discharge current, two process types may take place in the treatment area at the surface. At a low discharge current ($0.5 \le I \le 1$ mA; see curves 1 and 2), the plasma is observed to be deficient in negative oxygen ions because the concentration of neutral molecules in the process gas is low.

At $0.5 \le I \le 1$ mA, the mean free path of charged particles across the entire range of accelerating voltages reaches the value of the distance between the electrodes and the substrate surface [66].

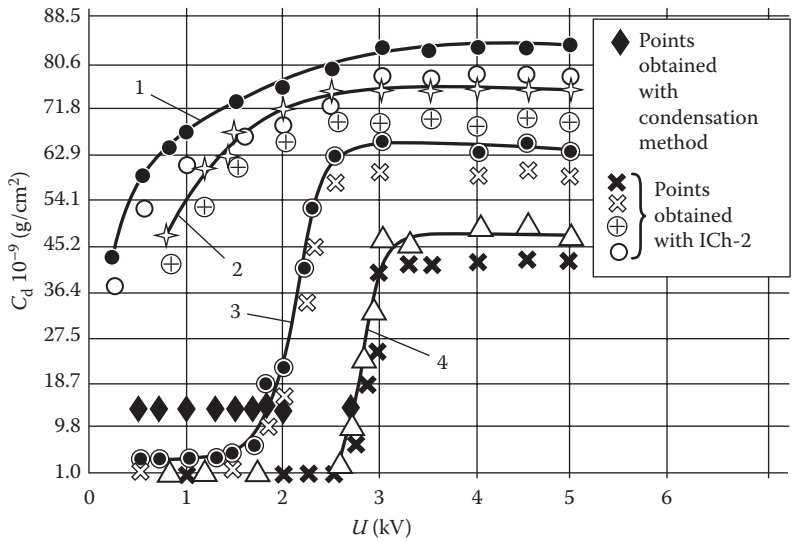


**FIGURE 3.15** Relationship between the degree of surface cleanliness and the accelerating voltage: (1) 0.5 mA, (2) 1 mA, (3) 2 mA, and (4) 3 mA. $t = 10$ s.

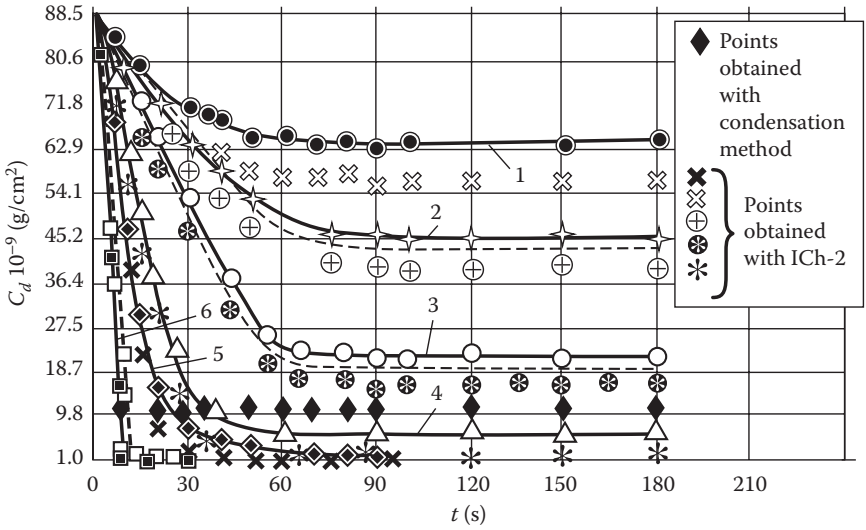


**FIGURE 3.16** Relationship between the degree of surface cleanliness and the irradiation time: (1) 0.5 mA ($t_{lim}$ = 65 s), (2) 1 mA ($t_{lim}$ = 60 s), (3) 1.4 mA ($t_{lim}$ = 50 s), (4) 1.5 mA ($t_{lim}$ = 30 s), (5) 2.6 mA ($t_{lim}$ = 20 s), and (6) 3 mA ($t_{lim}$ = 10 s). $U$ = 3 kV. Dashed lines indicate the relationship (3.22).

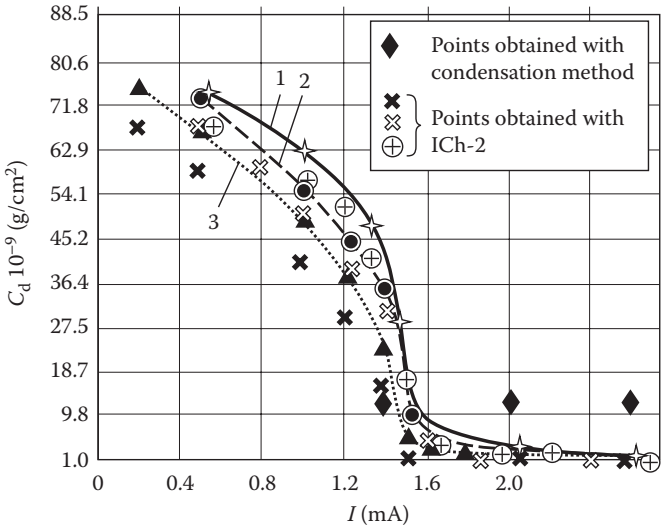


**FIGURE 3.17** Relationship between the degree of surface cleanliness and the discharge current at $U$ = 3 kV: (1) $t$ = 50 s, (2) $t$ = 60 s, and (3) $t$ = 120 s.

Negative oxygen ions interact with the layer of organic contaminants at energies that virtually equal $eU$. High-energy $O^-$ ions cause intense physical sputtering of the surface. But the ion flux and the neutral-molecule flux incident on the surface are not sufficient for forming the required quantity of chemically active oxygen radicals capable of intensifying the chemical reactions.

The physical-sputtering rate is notably higher than the rate of the chemical reactions. Sputtered modified atom–molecule complexes of organic contaminants are adsorbed back onto the surface and contaminate it. With an increase in the accelerating voltage, the energies of the particles bombarding the surface only increase, and there is an increased number of those sputtered atoms that for the most part do not undergo chemical reactions because of a lack of active O* radicals and thus increase the surface concentration of contaminants. It is this that explains the similar behaviors of curves 1 and 2 and the growth of $C_d$ across the entire range of accelerating voltages.

But curve 2 lies lower than curve 1. This is due to the large quantity of negative oxygen ions and neutral process-gas molecules in plasma (at $I = 1$ mA) and to the diminishing energies of the bombarding particles, resulting in a higher number of CAPs at the surface. CAPs react with the atom–molecule complexes of contaminants and impede their sputtering by diminishing $C_d$.

Analysis of curves 3 and 4 confirms these statements. At a discharge current of $I \geq 2$ mA, the number of CAPs at the surface is sufficient for the ion-chemical, ion-stimulated, and electron-stimulated etching of organic contaminants. The rate of the chemical reactions is comparable with or exceeds the physical-sputtering rate of organic contaminants. It is this that explains the minimum values of $C_d$ in the voltage ranges $0.5 \leq U \leq 1.2$ kV (curve 3) and $0.5 \leq U \leq 2.5$ kV (curve 4). At voltages of $1.2 \leq U \leq 2.5$ kV (curve 3) and $2.5 \leq U \leq 3$ kV (curve 4), the particle energy reaches a value at which the physical-sputtering processes begin to intensify, resulting in a drastic increase in the concentration of surface contaminants.

The saturation regions of curves 1, 2, 3, and 4 indicate that organic contaminants have been completely sputtered from the substrate surface. As the discharge current increases, a higher accelerating voltage must be applied to the gas-discharge device's electrodes to ensure the charged particles reach the surface with energies sufficient for contaminant molecules to be completely sputtered. As a result, curves 1, 2, 3, and 4 begin to become saturated at different accelerating voltages. Different saturation levels indicate that as the discharge current increases, some of the atom–molecule complexes contaminating the surface have time to be removed by the evacuation system as gaseous products through the mechanisms of ion-chemical etching, ion-stimulated etching, and electron-stimulated etching.

To select the optimal surface-cleaning regime (based on investigating its time dependence), we have obtained experimental curves that show the relationship between surface cleanliness and irradiation time, $C_d = f(t)$ (see Figure 3.16). The different slopes of the curves are due to the different quantities of CAPs reacting with contaminant atoms. Because low discharge currents correspond to the low fluxes of radicals and negative ions of oxygen incident on the surface, removing contaminants takes a longer time.

If there is a CAP deficiency, oxygen radicals will first react with chemically active hydrogen atoms. Removing chemically inert carbon atoms to a level of

$C_d = 10^{-9}$ g cm$^2$ is possible if the CAP deficiency at the substrate surface is eliminated. This, in turn, is possible at a discharge current of $I = 2.6$ mA and $I = 3$ mA. In the latter case, the irradiation time at which $C_d = 10^{-9}$ g/cm$^2$ is achieved is as little as 10 s. A long irradiation time at an accelerating voltage greater than 1 kV causes the substrate surface to heat to temperatures that impede the adsorption of neutral process-gas molecules and, therefore, the formation of CAPs [209]. Each value of the discharge current has its own critical irradiation time ($t_{\text{lim}}$), at which the surface heats up to a temperature at which neutral molecules are desorbed from it. The value of θ tends to zero in the region $t \geq t_{\text{lim}}$, thereby reducing the removal rate of organic contaminants at low currents. This explains the segments of curves 1, 2, 3, and 4 (Figure 3.16) in which the value of $C_d$ ceases to depend on plasma-treatment time. These segments can likely be explained as well by the presence of a hard-to-remove modified layer of carbon compounds whose removal requires high discharge currents. The value of $t_{\text{lim}}$ for each discharge current is determined by the intersection point of tangents to the appropriate curve (see Figure 3.16).

The relationship $C_d = f(I)$ in Figure 3.17 shows that for three different cleaning times, a sharp reduction in the contaminant concentration at the surface is observed for all curves in the range $1.4 \leq I \leq 1.6$ mA. The sharp decrease in the value of $C_d$ in this discharge-current range is due to the intense filling of the surface by chemically active O* radicals formed as a result of the ion and electron stimulation of neutral process-gas molecules as well as ion-chemical etching [209]. The CAP deficiency at the surface typical of lower discharge currents ($I \leq 1.4$ mA; see also Figure 3.15) begins to be eliminated. At $I \geq 2.6$ mA, $C_d$ reaches its minimum value, and this confirms that the CAP deficiency is fully eliminated.

AFM images showing the surface before (Figure 3.10) and after (Figure 3.18) final cleaning confirm that high-voltage gas-discharge off-electrode plasma efficiently removes organic contaminants from substrate surfaces.

If the initial surface has a contaminant film and shows hydrophobic properties (the interaction distance between the cantilever and the surface structure is a 3-nm

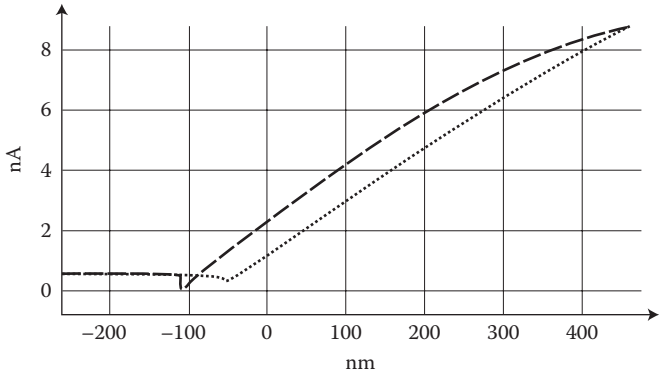


**FIGURE 3.18** Force curve obtained with Solver PRO-M for the test surface after final cleaning. The interaction distance between the cantilever and the surface structure is an $H_2O$ film, $H = 20$ nm.

film of organic contaminants; see Figure 3.10), after final cleaning, the surface shows hydrophilic properties and therefore actively adsorbs water. Because of capillary action [203,206], the layer thickness $H$ equals 20 nm. Therefore, the curve in Figure 3.18 characterizes a technologically clean surface because the surface is free from molecules of organic contaminants.

Thus, to attain the precision-cleanliness level, this monograph recommends cleaning substrate surfaces with high-voltage gas-discharge plasma at $U = 1.2$ kV, $I = 3$ mA, and $t = 10$ s.

The experimental contaminant concentrations were obtained with the tribometric method, which is discussed in Chapter 2. The method's reliability was confirmed by using the condensation method to take similar measurements with the ICh-2 tribometer (see Figures 3.15 through 3.17). The variance of the readings obtained from the methods under the same regimes was found to not exceed 10%. The higher concentrations obtained with the condensation method are due to its threshold sensitivity equal to $10^{-8}$ g/cm$^2$, while the low $C_d$ obtained with the ICh-2 tribometer is due to error caused by the probe breaking away from the surface, poor resistance reproducibility of the signal contacts, and friction in moving parts [109].

For comparison, Figure 3.16 shows the curves derived from expression (3.22). The close agreement between the curves and the experimental data shows that the proposed model adequately describes the process of physically cleaning organic contaminants off substrate surfaces with high-voltage gas-discharge off-electrode plasma. An important achievement is that using the proposed cleaning method in technology for fabricating subminiature relays for space applications and semiconductors helped improve the contact conductivity of the former [220] and the parameters of the latter, which were measured with the quick-measurement unit described in detail in Reference 221.

## 3.8 PROCEDURE FOR FINAL SURFACE CLEANING WITH OFF-ELECTRODE PLASMA

The procedure for final cleaning of substrate surfaces with off-electrode plasma consists of several consecutive steps that, once completed, yield a technologically clean surface (a surface with a cleanliness level of $10^{-9}$ g/cm$^2$). Coupled with vacuum techniques for mask deposition that are completed as part of a single cycle, this procedure helps fabricate microstructures with desired parameters.

When a mask is deposited through the thermal vacuum evaporation technique, the final-cleaning procedure is completed as part of that technique and comprises the following steps:

1. Placing chemically cleaned initial substrates on the substrate carousel in the vacuum chamber
2. Evacuating the vacuum chamber to a pressure of $7.5 \cdot 10^{-2}$ Torr with a mechanical pump; configuring the high-voltage gas-discharge device: setting the discharge current at 3 mA, the electrode voltage at 1.2 kV, and the irradiation time at 10 s (per substrate)

3. Cleaning the initial substrates under these conditions with a low-temperature plasma flux to a level of $10^{-9}$ g/cm$^2$
4. Deactivating the high-voltage gas discharge
5. Depressurizing the working chamber
6. Removing the substrates from the carousel and placing them in the desiccator or the tribometer

This final-cleaning procedure makes it possible to obtain a technologically clean surface.

## 3.9 CHAPTER SUMMARY

The existing methods for cleaning substrate surfaces have several major drawbacks:

- The methods cause surface defects in the form of craters and wavelike relief.
- HF and SHF discharge parameters that are difficult to stabilize and the loading effect undercut efficiency.
- The equipment used is complex, energy-intensive, and expensive.

Our investigations based on the proposed gas-discharge devices enable us to propose efficient methods for fabricating surfaces with the desired properties, including a surface-cleaning method. We have experimentally proved that the cleaning method yields a surface with a cleanliness level of $10^{-9}$ g/cm$^2$ and stands out from the others thanks to its low cost and energy consumption.

The results we obtained can be used in technology for fabricating DOEs and nano- and microelectronic elements.